Superconductivity in Pb cluster assembled systems with different degrees of coagulation

J. Cuppens, C. P. Romero, P. Lievens, and M. J. Van Bael[*]

Laboratory of Solid-State Physics and Magnetism and INPAC, K.U. Leuven, Celestijnenlaan 200D, 3001 Leuven, Belgium
(Received 3 July 2009; published 26 February 2010)

Superconducting properties are observed and investigated in Pb nanogranular systems prepared by deposition of clusters produced in a laser vaporization cluster source. Different morphologies were achieved by controlling the degree of coagulation via the substrate temperature and the magnetic response of these systems was studied. Deposition on substrates at temperatures above 200 °C results in an ensemble of weakly coupled islands showing superconducting confinement effects. Cluster deposition on cooled substrates limits the coagulation and results in cluster assembled thin films with strong intergrain coupling. This method provides a unique way to produce systems with very high flux pinning leading to avalanche effects.

PACS number(s): 74.25.Ha, 62.23.St, 81.16.−c, 73.22.−f

I. INTRODUCTION

As individual nano-objects with sizes bridging the atomic and the submicron scales, clusters have unique structural,[1,2] electronic,[3,4] optical,[5] magnetic,[6,7] and superconducting[8,9] properties, which are being studied in the gas phase as well as deposited on substrates. The use of preformed clusters as building blocks for nanostructured cluster assembled systems moreover offers promising possibilities for exploiting these interesting new features.[10] The self-assembly of nanoclusters into a system with distinct morphology provides a bottom-up alternative to top-down nanopatterning methods (e.g., lithography), allowing to investigate and control new properties in nanostructured materials, which may in some cases show reminiscence of the properties of their building blocks.[11]

Confinement effects in nanostructured superconductors have been studied intensively in top-down patterned systems, with typical length scales in the (sub)micron range.[12,13] As superconducting objects assume sizes comparable to their characteristic length scales λ and ξ (the magnetic penetration depth and the coherence length, respectively) their properties will change. For example, due to incomplete screening of the external magnetic field the critical magnetic field in small superconductors may become considerably larger than in bulk.[14,15]

Superconducting particles or grains are moreover used as constituents of granular superconducting systems. Important parameters in such granular systems are the intergrain coupling energy and the charging energy of a single grain. Superconductivity can be intragranular for small intergrain coupling energy (the grains behave as individual particles) or intergranular if the coupling is sufficiently large. In granular superconducting systems, interesting properties have been studied such as the disorder-driven superconductor-insulator transitions,[16–19] critical currents in arrays of Josephson junctions,[20] percolation,[21] and magnetoresistance.[22] In these previous studies, the focus was mainly on electrical transport properties studied through temperature-dependent electrical resistivity and magnetoresistance measurements.

Different techniques have been used in the past to produce superconducting grains and granular systems, such as molecular-beam deposition,[16,17] (in combination with) quench condensation, magnetron sputtering,[23] as well as chemical formation of, e.g., Pb particles in a porous membrane by reduction in a Pb salt.[24] In most reported investiga-

tions of granular superconducting systems, the grain-size distribution, the order of the system, and the coupling between the grains are typically varied by using the coverage (or concentration or film thickness) as a control parameter[22] determining the systems properties.

Here we present an interesting way of building granular superconducting systems by using gas-phase clusters as building blocks, and by controlling the size and coupling between the grains via coagulation, hence leaving the coverage or film thickness fixed. We have selected Pb as superconducting material which has a bulk critical temperature T_c of 7.2 K. Moreover, the relatively low bulk melting temperature for Pb(T_m=327.46 °C) makes coagulation of the clusters after deposition on the substrate more likely. In nanoscale clusters, the melting temperature will even be considerably lower.[25,26] The use of a laser vaporization cluster source and subsequent low-energy cluster beam deposition for the production of cluster assembled superconducting Pb systems provides additional control on the nanoscale structure of these samples.[27] We demonstrate how the final grain size and coupling are controlled via coagulation of the clusters through the substrate temperature upon deposition.

In order to study the superconducting state in these systems and the influence of the granular morphology, we have focused on the overall magnetic response which gives information on the superconducting screening and magnetic-flux penetration. These properties are much less studied in granular superconducting systems in comparison to electrical transport properties that have been broadly studied in the past. The magnetic response allows us to also study ensembles of electrically uncoupled islands.

II. EXPERIMENT

Pb clusters were produced in a dual-target dual-laser vaporization setup, which basically consists of three differentially pumped ultrahigh-vacuum chambers: source, extraction, and deposition chamber. The clusters are produced in the source chamber by a combination of laser vaporization, gas aggregation, and dynamic expansion, which is achieved by placing the laser vaporization source between a pulsed gas valve and a divergent nozzle. In the source, a Pb target is ablated by two Nd:YAG lasers with a wavelength of 532 nm and a pulse width of 7 ns. In a small formation volume,
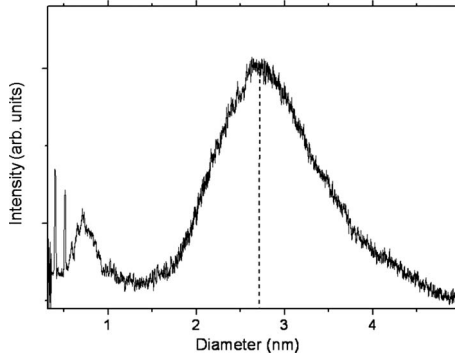
FIG. 1. Size distribution of Pb clusters in the beam, inferred from the time-of-flight mass spectrum.

the produced plasma is cooled by 125 μs pulses of ultrapure He carrier gas from the gas valve (PSV, R. M. Jordan Co., Inc., operated at 10 Hz), allowing cluster formation via condensation and aggregation. The mixture of gas, atoms, and clusters expands into the vacuum of the extraction chamber through the nozzle where cluster formation comes to an end. The cluster beam is taken by the carrier gas from the extraction chamber through a skimmer into the deposition chamber. In the extraction chamber, charged clusters can be accelerated by an electrical potential on a set of extraction plates, which allows the cluster size distribution to be monitored with a time-of-flight mass spectrometer. Upon entry into the ultrahigh-vacuum deposition chamber (base pressure 1.2×10^{-9} bar), the clusters are deposited at low energies (<0.5 eV/atom) on a substrate. More details about the setup can be found elsewhere.[28,29] The clusters were produced with the source cooled to a low temperature of -100 °C with liquid nitrogen. It was found that this cooling of the source enhances the cluster formation process and leads to a larger average diameter of the produced clusters. The cluster size distribution in the beam was monitored with a time-of-flight mass spectrometer. The mass abundance spectrum for Pb clusters can be converted into a size distribution (see Fig. 1) by assuming spherical clusters and the Wigner-Seitz radius of bulk Pb. The distribution shows an average cluster diameter of 2.7 nm (310 atoms) and a width of 1.5 nm at half the maximum value. The sharp peaks and small bump at sizes below 1 nm correspond to Pb atoms, dimers, and small clusters, which constitute a negligible volume fraction.

SiO_2 substrates were used for the deposition and were kept at fixed temperatures varying between -70 and 600 °C by thermal contact of the substrate with a heated or cooled copper block. The thickness of the deposited cluster layer was monitored using a quartz microbalance and was about 20 nm for all samples mentioned. A thin capping layer of Pd (3 nm) was added using an *in situ* e-beam evaporator in the deposition chamber as a protection against immediate oxidation during transport between deposition setups. The sample was subsequently covered with a 20 nm Si layer by e-beam evaporation in another UHV chamber while the substrate was maintained at room temperature. The samples produced at high substrate temperature were slowly cooled down to room temperature after cluster deposition, prior to the Pd

deposition. For those samples where the Pb clusters are deposited on cooled substrates, the Pd layer was also deposited at low temperature.

By adding a Pd capping layer, the samples were found to be more likely to show global superconducting behavior. The influence of the Pd capping layer is twofold. First, as mentioned above, the Pd prevents the Pb layer from oxidation during the short ambient exposure (a few minutes) before the Si capping layer is deposited. Second, the metallic Pd layer may enhance the long-range superconducting order in the granular film. More specifically the proximity effect results in a better coupling between the grains via the weak order parameter induced in the metallic Pd overlayer, enabling global superconductivity especially for samples produced at low temperature (see below). This effect was demonstrated by Frydman *et al.*[30] for quench condensed granular superconductors. By adding a normal-metal overlayer to isolated Pb grains the long-range order in the film could be enhanced, resulting in a crossover from insulating to superconducting behavior.

The samples were characterized by atomic force microscopy (AFM), x-ray diffraction (XRD), and Rutherford backscattering spectroscopy (RBS). XRD patterns were recorded in grazing incidence as well as in θ-2θ configuration with a PANalytical X'Pert PRO x-ray diffractometer using Cu $K\alpha1$ radiation. The used AFM is a Digital Instruments Dimension system. The superconducting properties of the produced systems were investigated using superconducting quantum interference device magnetometry (Quantum Design MPMS-XL).

III. MORPHOLOGY

In this section, we describe the morphology of the layers formed by deposition of Pb clusters. The preformed Pb clusters are deposited on SiO_2 substrates with their inherently low kinetic energy (<0.5 eV/atom) so that cluster *fragmentation* upon impact on the substrate is unlikely to occur.[31] The morphology of the resulting cluster assembled system is hence controlled by cluster-surface and cluster-cluster interactions, more specifically *diffusion* and *coalescence*.[32] Below we argue that the morphology of the Pb cluster assembled layers is mainly determined by coalescence, which largely can be regulated via the substrate temperature T_{subs}.

Before discussing the role of T_{subs}, it should be noted that the cluster flux reaching the surface is not continuous but chopped as a consequence of the pulsed nature of the deposition process. With a pulse duration of the helium carrier gas of $\sim$125 μs and the chopping frequency being 10 Hz, approximately 0.02 atomic layers are deposited per pulse.

The clusters are produced in a cooled (-100 °C) source but will thermalize with the substrate ($-70 < T_{subs} < 600$ °C) upon deposition and we may therefore assume that the cluster temperature is determined by T_{subs} and the substrate temperature will hence determine the degree of diffusion and coalescence.

The importance of *diffusion* in our systems is limited to the initial stages of the growth; only then diffusion is required for the clusters to interact. After the initial stage, once
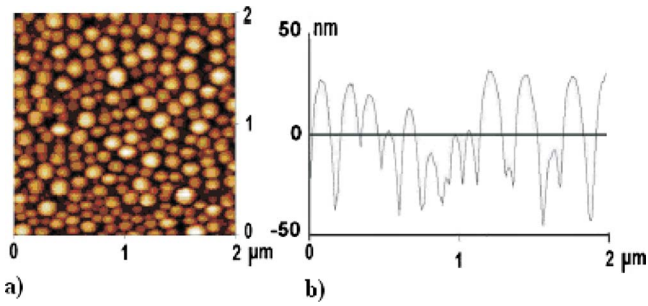
FIG. 2. (Color online) (a) 2×2 μm^2 AFM image of sample PbA deposited at $T_{subs} = 600$ °C. The color scale spans 100 nm. (b) Section of AFM image of sample PbA.

FIG. 3. (Color online) (a) 2×2 μm^2 AFM image of sample PbB deposited at $T_{subs} = -70$ °C. The color scale spans 10 nm. (b) Section of AFM image of sample PbB taken across an artificial scratch on the sample.

the substrate is covered, clusters will land on the deposits already present and diffusion is no longer relevant. For a given material and substrate, the diffusion coefficient increases with increasing temperatures. As a consequence the cluster diffusion length on a hot substrate will be considerably larger than on a cold one.

Coalescence is also strongly temperature dependent and is the most important factor determining the morphology of the cluster assembled Pb layers. Substrate temperatures above the melting point, on one hand, will yield liquid Pb nanodroplets on the surface. When these droplets meet by diffusion on the surface or when additional clusters land onto existing droplets, liquid-liquid coalescence of the "hot" clusters will lead to bigger droplets by three-dimensional (3D) growth. Subsequent cooling down of the resulting system leads to recrystalization of droplets into semispherical nanoislands. On the other hand, when clusters are deposited on cooled substrates, the initial growth process will consist of limited diffusion of clusters on the uncovered substrate. When these "cold" clusters meet they will form a larger entity by juxtaposition and partial coalescence. This will promote the two-dimensional growth of a granular layer.[33,34] Intermediate substrate temperatures will lead to a combination of the above with stronger coalescence as the temperature increases.

Several samples were produced at different substrate temperatures: −70, 40, 200, 400, and 600 °C. Figure 2(a) shows an AFM image for a sample produced at 600 °C (PbA). All samples are covered by a Si capping layer but the image clearly shows the underlying ensemble of small islands that are formed by strong coalescence of the clusters on the hot substrate. A cross section is shown in Fig. 2(b). It can be seen that surface tension has shaped the 3D islands into semispherical droplets with an average diameter of 116 ± 30 nm and an average height of 56 ± 15 nm. Samples deposited at 200 and 400 °C show a similar island structure although as T_{subs} decreases, the islands are found to deviate more from a semispherical shape and they are more plateau like with flattened top surfaces.[35] This suggests that at the highest $T_{sub} = 600$ °C $> T_m$, the islands grow by coalescence only while at lower substrate temperatures the islands are formed by a combination of coalescence and juxtaposition of the clusters.

In contrast, the Pb clusters deposited on cooled (−70 °C) substrates form a smoother layer as can be seen in Fig. 3, with rms roughness of 2 nm on a 2×2 μm^2 area.
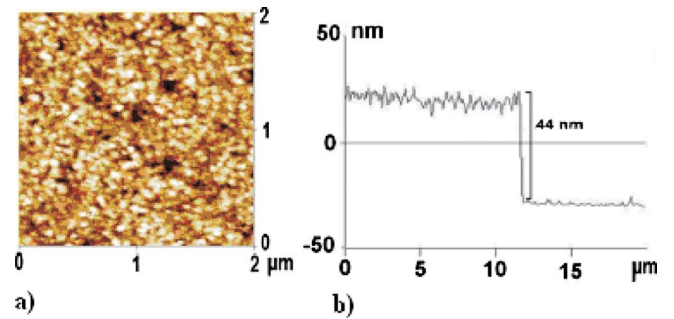
Although the imaged top surface is that of the Si capping layer and can in this case not directly be related to the morphology of the underlying Pb cluster film, it is clear that there are no pronounced islands formed and the Pb clusters form a rather smooth cluster assembled layer. Due to the substrate temperature being far below the melting temperature of the clusters, coalescence is much slower. The degree of coalescence can be established from the size of the Pb grains in the resulting layer. A grain size of around 20 nm was estimated by x-ray diffraction via the width of the Bragg peaks using the Scherrer law,[36] referring to the direction perpendicular to the Si surface. With the initial average cluster size being 2.7 nm a grain size of 20 nm indicates that coalescence still plays a role in the growth process even at the lowest substrate temperatures. Coalescence and island formation was also observed in atomic-vapor-deposited quenched condensed Pb layers with substrate temperatures below 20 K.[17] The total thickness of the layer was determined by an AFM measurement on a scratch reaching down to the substrate [Fig. 3(b)], revealing 44 nm in very good correspondence with the 20 nm Pb cluster assembled layer, 3 nm Pd capping and 20 nm Si capping. This was also verified using RBS measurements. For all samples XRD θ-2θ data (not shown) indicated that the fcc(111) growth direction was dominant. No traces of Pb oxide were found in the XRD patterns and RBS spectra.

IV. SUPERCONDUCTING PROPERTIES

A. Ensemble of superconducting islands

By varying the substrate deposition temperature, the morphology of the deposited Pb cluster layers evolves from individual nanoislands (strong coalescence, sample PbA) to granular films (weak coalescence, sample PbB). In this section, we describe the superconducting properties of the films composed of individual superconducting islands as obtained with cluster deposition at elevated temperatures. When scaling down a superconducting particle to sizes on the order of 100 nm, comparable with the characteristic length scales ξ and λ, its properties will be affected. The superconducting phase boundary was constructed from measurements of the magnetization as a function of temperature, $M(T)$, at differ-
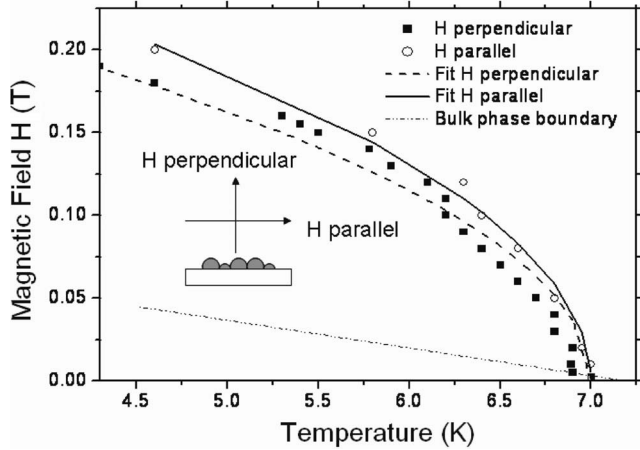
FIG. 4. Phase boundary of sample PbA: nanoscale islands produced through cluster deposition at $T_{\text{subs}} = 600\ ^{\circ}\text{C}$. The experimental data are fitted with a square-root dependence ($\propto \sqrt{1 - T/T_c}$). For comparison the bulk Pb phase boundary is also included in the figure.

ent fixed magnetic fields H. The onset of a diamagnetic response indicates the transition to the superconducting phase and the onset temperature was identified as the critical temperature $T_c(H)$. From the different $T_c(H)$ data points, the critical field as a function of temperature $H_c(T)$ is constructed. Figure 4 shows the superconducting phase boundary for sample PbA for the magnetic field applied perpendicular and parallel to the substrate plane. All $M(T)$ curves showed a paramagnetic background proportional to H/T which needed to be subtracted in order to clearly identify the onset of the diamagnetic response.

The critical temperature at zero field is slightly below the bulk value, which is a consequence of the proximity effect induced by the thin Pd layer. Hsu *et al.* have studied the crossover in the superconducting behavior from individual isolated grains to a continuous "dirty" type II superconducting film (with mean-free path $l \ll \xi_0$) by increasing the concentration of metallic grains in an insulating matrix. Based on a model for Josephson-junction arrays with weakly coupled spherical grains, the temperature dependence of the critical field $H_{c2}(T)$ can be written as[37,38]

$$H_{c2}^2(T) = \frac{5}{3}\left(\frac{\phi_0}{2\pi\xi_{gr}R}\right)^2\left(1 - \frac{2\xi_{gr}}{t^2}\right) \qquad (1)$$

with ξ_{gr} the coherence length for a single grain, R the radius of a spherical grain, and t a parameter representing the intergrain coupling; t diverges for weak coupling while it will be small for stronger coupling. In the extreme case where the grains are fully coupled, the system behaves as a dirty type II superconducting film with a linear temperature dependence of $H_{c2}(T)$. The square-root dependence of the critical field as shown in Fig. 4 indicates that the coupling between the particles is very weak. This can be inferred from Eq. (1), where for diverging t, a square-root dependence of the critical field is found corresponding to the behavior of isolated nanograins.[37]

Also clear from Fig. 4 is that due to their confined geometry, the critical field of these nanoislands is much larger than in bulk Pb. This can be understood because the screening of the magnetic field is not complete in small particles so that, at a given field, less energy is spent for screening the magnetic field compared to a bulk system with complete screening.[14] Therefore higher magnetic fields can be applied before the superconducting state becomes energetically unfavorable and the nanoislands turn to the normal metallic state. The observation that the phase boundaries for parallel and perpendicular magnetic fields are very similar also supports the conclusion that there is no coupling between the islands. If there were coupling between the islands, the phase boundary for the two field geometries would be different because of the different confinement geometry. Indeed, in perpendicular field, the screening currents generating the diamagnetic response would extend over multiple islands whereas for parallel field they would be confined by the island height. In contrast, the phase boundaries for parallel and perpendicular fields are almost identical (see Fig. 4). The critical field in the parallel direction is only slightly higher than in the perpendicular direction. This can be attributed to the shape anisotropy of the semispherical islands which have a diameter of about twice the height. This means that superconductivity will be more confined perpendicular to the substrate which is reflected in the phase boundary for parallel field. Using formula (1) for diverging t and with the coherence length $\xi(0) = 30$ nm, which is a typical value for dirty type II Pb films (see, for example, in Ref. 39), we can calculate the size of the superconducting grains from the phase boundaries. From the parallel field phase boundary, we find an island height of 80 nm while from the perpendicular field phase boundary, we estimate a diameter of 110 nm. Both values are in good correspondence with the respective AFM results shown above, supporting our conclusion that the islands behave as uncoupled superconducting particles. It should be noted that the extremely thin Pd (3 nm) layer between the Pb islands and the Si capping layer will be highly discontinuous as it is grown on the rough island layer and will in this case not provide any coupling between neighboring islands.

The magnetization as a function of applied magnetic field (perpendicular to the substrate plane) for sample PbA at $T = 4$ K is given in Fig. 5 for increasing as well as decreasing field. The full measurement was performed in a field range from -0.5 to 0.5 T. A fully reversible $M(H)$ behavior is found for this system of Pb islands, consistent with the magnetization of individual decoupled small particles. No hysteresis can be observed because it is impossible for the magnetic flux to be trapped in such a small particle. Similar behavior was found in Ref. 24 for Pb nanoparticles embedded in a porous membrane prepared by reduction in a Pb salt.

B. Superconducting cluster assembled thin films

While the properties of individual superconducting particles have already been addressed in several studies,[9,14,23,24] the magnetic response of cluster assembled superconducting systems have received less attention. In the following, we show that the bottom-up assembly of clusters into a cluster
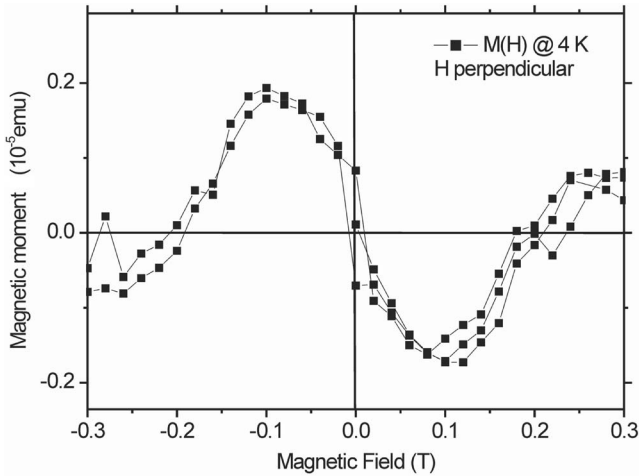
FIG. 5. Magnetization as a function of the magnetic field for sample PbA at T=4 K.

assembled superconducting layer provides a very efficient way to achieve very strong flux pinning in superconducting Pb films.

The superconducting phase boundary for sample PbB produced at a substrate temperature of −70 °C is shown in Fig. 6. This cluster assembled film reveals a linear temperature dependence of H_{c2} over a broad temperature interval near T_c. This corresponds with the behavior of a dirty type II superconductor with

$$H_{c2}(T) = \frac{\phi_0}{2\pi\xi(T)^2} \quad \text{and} \quad \xi(T) = 0.855\sqrt{\frac{\xi_0 l}{1 - T/T_c}}, \quad (2)$$

where ϕ_0 is the superconducting flux quantum, ξ_0 the intrinsic BCS coherence length (ξ_0=83 nm for bulk Pb), T_c the zero-field critical temperature, and l the elastic mean-free path. A thin Pb film with $l \ll \xi_0$ is known to behave as a dirty type II superconductor. Assuming that Eq. (2) can be applied to this cluster layer, we find a coherence length $\xi(0)$ =47 nm and a mean-free path l=36 nm. The mean-free path
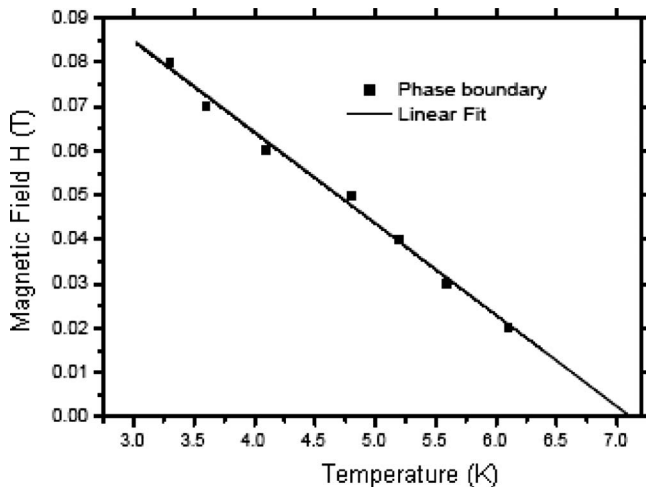

FIG. 6. Phase boundary of sample PbB. The linear behavior corresponds to the dirty type II nature of the film.

l of 36 nm is much larger than the size of the deposited clusters and is even larger than the grain size (perpendicular to the substrate) of the resulting layer as found by XRD (see above). This again illustrates the important role of cluster coalescence in the growth process even at the lowest substrate temperatures.

While the nanoisland system (see previous section) was characterized by reversible $M(H)$ magnetization behavior and the absence of flux trapping in individual islands, it will be particularly interesting to investigate the flux pinning in this type II superconducting system built by cluster deposition. In an applied field, magnetic flux can enter a type II superconductor as quantized flux lines. The movement of these flux lines, driven, e.g., by an electrical current or thermal excitations, causes dissipation. Flux pinning at defects and the ways to enhance it are therefore intensively studied. By optimizing the pinning strength, the critical current density (j_c) of the superconductor can be strongly increased. The pinning force and j_c can be enhanced by introducing artificial pinning centers such as antidots [(sub)micron-sized holes] or magnetic dots via top-down methods or by introducing point defects or impurity phases (top down or bottom up).[40–42]

Figure 7 shows the magnetization as a function of the applied field of the cluster assembled thin-film PbB in comparison with a reference Pb layer of equal size grown by molecular-beam deposition. It can immediately be seen that this magnetization behavior is highly hysteretic in contrast to Fig. 5, indicating the strong pinning of magnetic flux in the sample as the magnetic field is swept. Moreover, the width of the hysteresis loop of the cluster assembled sample is more than an order of magnitude larger than that of the reference film, reflecting a huge increase in the pinning strength.

With the critical state model, we can estimate the critical current density from the width of the magnetization loop and the dimensions of the sample.[43] For the cluster assembled film, we find $j_c \sim 3.4 \times 10^7$ A/cm^2 at 6 K which is four times larger than for an molecular-beam epitaxy (MBE)-grown thin film and of the same order as a film with artificially introduced pinning centers.[41] The increase in pinning force should be directly related to the granular internal structure of the film. The mean-free path and grain size of a textured reference layer grown by MBE are comparable to the one we find for the cluster assembled layer. Nevertheless the pinning efficiency in the cluster assembled film is much stronger, which indicates that the microscopic details of the morphology and, in particular, the intergranular regions are determining the unique pinning properties of these cluster assembled films. Another interesting observation in Fig. 7 is the presence of irregular jumps in the magnetization that can be seen at lower temperatures. These are flux jumps resulting from thermomagnetic instabilities, also called flux avalanches.[44] The origin of these avalanches is related to the strong flux gradient or steep flux density profile that can exist in samples with strong pinning. The Bean critical state model in its simplest form assumes that an equilibrium between the pinning force and the external magnetic pressure results in a constant flux gradient.[43] Like a sand hill the flux configuration is in a metastable equilibrium and can change to a new lower-energy configuration when permitted.[44] To obtain the new energy configuration, the system may develop flux
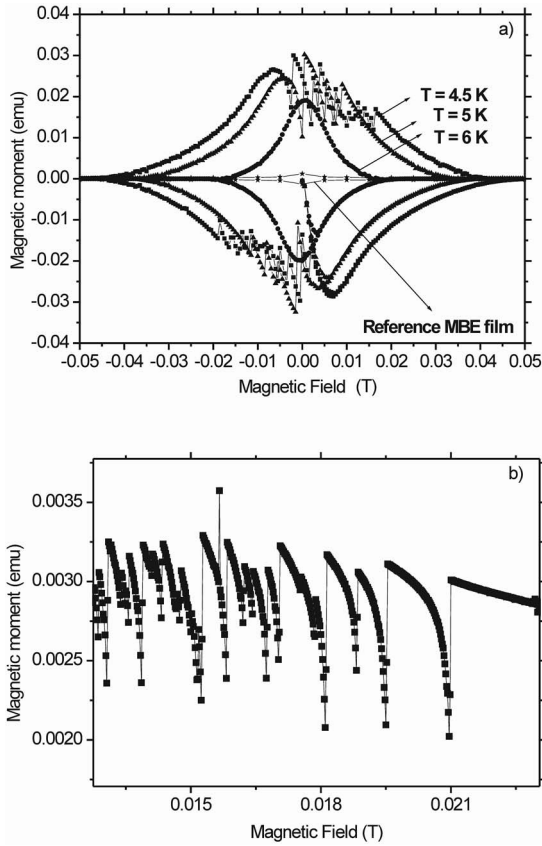
FIG. 7. (a) Magnetization loop of sample PbB at 4.5, 5, and 6 K. The magnetization of an MBE reference film at 4.5 K is also shown in comparison. (b) Detail of the magnetization as a function of field at $T = 3.5$ K for a Pb cluster assembled sample produced at low substrate temperature showing flux avalanches.

FIG. 8. H-T diagram marking the region where vortex avalanches occur in PbB in comparison with a Pb film with artificial pinning sites (data from Ref. 44) and a continuous reference Pb film grown by MBE.

creeps, where thermal and quantum fluctuations help to overcome the pinning barrier.[45] The dissipative motion of these flux lines will locally increase the temperature and therefore decrease the pinning strength and promote the depinning of additional flux lines. Eventually this will result in flux avalanches showing up as jumps of the magnetization. Similar flux avalanches have been observed in high-pinning samples at low temperatures and magnetic fields, where the flux-pinning strength is maximal.[44,46] Figure 8 shows the field and temperature region where flux avalanches are observed. The avalanche region is shown (dashed area) for the cluster assembled film PbB in comparison to a reference Pb MBE-grown textured film and a Pb film with artificial pinning centers (a periodic array of antidots introduced by lithography).[47] It is clear that the H-T region in which instabilities occur is much larger than for a reference MBE film and comparable to one with artificial pinning centers. Figure 7(b) shows a detail of the $M(H)$ curve of a sample produced at low temperatures showing vortex avalanches. This clearly reveals how the avalanches become more frequent at lower fields, i.e., deeper in the instability region shown in Fig. 8.

V. CONCLUSION

Deposition of Pb clusters produced in a laser vaporization cluster source results in superconducting systems with dis-
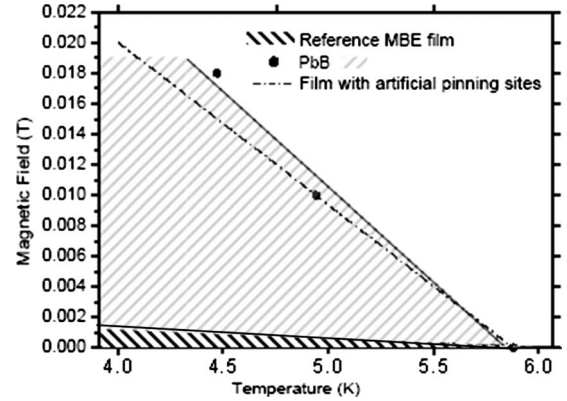
tinct properties depending on their morphology. The morphology (grain size and coupling) was manipulated by controlling the degree of coalescence via the substrate temperature upon deposition. For two different types of systems, deposited at high and low temperatures, the superconducting screening and magnetic-flux penetration was investigated by magnetization measurements.

High-substrate temperature deposition results in strong coalescence and provided a bottom-up way for the creation of an ensemble of nanoislands behaving as individual superconducting particles with sizes on the order of 100 nm with strongly enhanced critical fields.

Cluster assembled films with remarkably high flux pinning are created after deposition on cooled substrates where coalescence is less prominent. Pinning strength and critical current densities comparable to those of superconducting films with artificial pinning arrays were achieved without any top-down lithography, proving the power of this method as a viable bottom-up way to produce high-pinning thin films. The nature of the intergrain coupling and pinning mechanism requires further investigation. While this experiment focused on a strongly coalescing material, other materials with higher bulk melting temperatures will show less coalescence and will allow the study of superconducting properties of granular systems consisting of building blocks of only a few nanometers in size. Ultimately, the superconducting properties of individual clusters should be studied after deposition of individual clusters on a substrate.[48]

*Corresponding author.

[1] S. Bulusu, X. Li, L.-S. Wang, and X. C. Zeng, Proc. Natl. Acad. Sci. U.S.A. **103**, 8326 (2006).

[2] K. Sattler, *Cluster Assembled Materials* (Trans Tech, Zürich, 1996).

[3] H. Imamura, J. Chiba, S. Mitani, K. Takanashi, S. Takahashi, S. Maekawa, and H. Fujimori, Phys. Rev. B **61**, 46 (2000).

[4] D. C. Ralph, C. T. Black, and M. Tinkham, Phys. Rev. Lett. **74**, 3241 (1995).

[5] Y. Xia, B. Gates, Y. Yin, and Y. Lu, Adv. Mater. (Weinheim, Ger.) **12**, 693 (2000).

[6] M. Jamet, M. Jamet, W. Wernsdorfer, C. Thirion, D. Mailly, V. Dupuis, P. Mélinon, and A. Pérez, Phys. Rev. Lett. **86**, 4676 (2001).

[7] R. Moro, X. Xu, S. Yin, and W. A. de Heer, Science **300**, 1265 (2003).

[8] P. W. Anderson and S. H. Suhl, Phys. Rev. **116**, 898 (1959).

[9] C. T. Black, D. C. Ralph, and M. Tinkham, Phys. Rev. Lett. **76**, 688 (1996).

[10] M. Holdenried and H. Micklitz, Eur. Phys. J. B **13**, 205 (2000).

[11] J. Schmelzer, Jr., S. A. Brown, A. Wurl, M. Hyslop, and R. J. Blaikie, Phys. Rev. Lett. **88**, 226802 (2002).

[12] L. F. Chibotaru, J. Math. Phys. **46**, 095108 (2005).

[13] Y. Bruynseraede, L. Gielen, C. Strunk, G. Neuttiens, L. Stockman, C. Van Haesendonck, and V. V. Moshchalkov, Nanostruct. Mater. **6**, 169 (1995).

[14] J. A. A. J. Perenboom, P. Wyder, and F. Meier, Phys. Rep. **78**, 173 (1981).

[15] A. M. Clogston, Phys. Rev. Lett. **9**, 266 (1962).

[16] H. M. Jaeger, D. B. Haviland, B. G. Orr, and A. M. Goldman, Phys. Rev. B **40**, 182 (1989).

[17] K. L. Ekinci and J. M. Valles, Jr., Phys. Rev. Lett. **82**, 1518 (1999).

[18] V. M. Vinokur, T. I. Baturina, M. V. Fistul, A. Y. Mironov, M. R. Baklanov, and C. Strunk, Nature (London) **452**, 613 (2008).

[19] Y. Imry and M. Strongin, Phys. Rev. B **24**, 6353 (1981).

[20] G. Sambandamurthy, K. Das Gupta, V. H. S. Moorthy, and N. Chandrasekhar, Solid State Commun. **115**, 427 (2000).

[21] G. Deutscher, O. Entin-Wohlman, S. Fishman, and Y. Shapira, Phys. Rev. B **21**, 5041 (1980).

[22] I. S. Beloborodov, A. V. Lopatin, K. B. Efetov, and V. M. Vinokur, Rev. Mod. Phys. **79**, 469 (2007), and references therein.

[23] S. Bose, P. Raychaudhuri, R. Banerjee, P. Vasa, and P. Ayyub, Phys. Rev. Lett. **95**, 147003 (2005).

[24] S. Reich, G. Leitus, R. Popovitz-Biro, and M. Schechter, Phys. Rev. Lett. **91**, 147001 (2003).

[25] S. Hendy, S. A. Brown, and M. Hyslop, Phys. Rev. B **68**, 241403 (2003).

[26] F. Ercolessi, W. Andreoni, and E. Tosatti, Phys. Rev. Lett. **66**, 911 (1991).

[27] A. Perez, P. Melinon, V. Dupuis, P. Jensen, B. Prevel, J. Tuaillon, L. Bardotti, C. Martet, M. Treilleux, M. Broyer, M. Pellarin, J. L. Vaille, B. Palpant, and J. Lerme, J. Phys. D **30**, 709 (1997).

[28] W. Bouwen, P. Thoen, F. Vanhoutte, S. Bouckaert, F. Despa, H. Weidele, R. E. Silverans, and P. Lievens, Rev. Sci. Instrum. **71**, 54 (2000).

[29] A. N. Dobrynin, D. N. Ievlev, C. Hendrich, K. Temst, U. Hörmann, J. Verbeeck, G. Van Tendeloo, A. Vantomme, and P. Lievens, Phys. Rev. B **73**, 245416 (2006).

[30] A. Frydman, L. M. Merchant, and R. C. Dynes, Phys. Status Solidi B **218**, 173 (2000).

[31] C. Binns, Surf. Sci. Rep. **44**, 1 (2001).

[32] C. Bréchignac, Ph. Cahuzac, F. Carlier, C. Colliex, M. de Frutos, N. Kébaïli, J. Le Roux, A. Masson, and B. Yoon, Eur. Phys. J. D **16**, 265 (2001).

[33] L. J. Lewis, P. Jensen, and J.-L. Barrat, Phys. Rev. B **56**, 2248 (1997).

[34] P. Jensen, Rev. Mod. Phys. **71**, 1695 (1999).

[35] See supplementary material at http://link.aps.org/supplemental/10.1103/PhysRevB.81.064517 for samples produced with T_{subs} = 200 °C and 400 °C.

[36] H. P. Klug and L. E. Alexander, *X-Ray Diffraction Procedures*, 2nd ed. (Wiley, New York, 1974).

[37] S.-Y. Hsu and J. M. Valles, Jr., Phys. Rev. B **47**, 14334 (1993).

[38] G. Deutscher, O. Entin-Wohlman, and Y. Shapira, Phys. Rev. B **22**, 4264 (1980).

[39] A. V. Silhanek, L. Van Look, R. Jonckheere, B. Y. Zhu, S. Raedts, and V. V. Moshchalkov, Phys. Rev. B **72**, 014507 (2005).

[40] S. H. Nalwa, *Handbook of Nanostructured Materials and Nanotechnology* (Academic, San Diego, 2000) (and references therein).

[41] M. Baert, V. V. Metlushko, R. Jonckheere, V. V. Moshchalkov, and Y. Bruynseraede, Phys. Rev. Lett. **74**, 3269 (1995).

[42] M. J. Van Bael, K. Temst, V. V. Moshchalkov, and Y. Bruynseraede, Phys. Rev. B **59**, 14674 (1999).

[43] C. P. Bean, Phys. Rev. Lett. **8**, 250 (1962).

[44] E. Altshuler and T. H. Johansen, Rev. Mod. Phys. **76**, 471 (2004).

[45] P. W. Anderson, Phys. Rev. Lett. **9**, 309 (1962).

[46] S. Hébert, L. Van Look, L. Weckhuysen, and V. V. Moshchalkov, Phys. Rev. B **67**, 224510 (2003).

[47] A. V. Silhanek, S. Raedts, and V. V. Moschalkov, Phys. Rev. B **70**, 144504 (2004).

[48] K. Schouteden, A. Lando, E. Janssens, C. Van Haesendonck, and P. Lievens, New J. Phys. **10**, 083005 (2008).